Deep *in vivo* two-photon microscopy with a low cost custom built mode-locked 1060 nm fiber laser

Evan P. Perillo, Justin E. McCracken, Daniel C. Fernée, John R. Goldak, Flor A. Medina, David R. Miller, Hsin-Chih Yeh, and Andrew K. Dunn[*]

Department of Biomedical Engineering, The University of Texas at Austin, 107 W. Dean Keeton C0800, Austin, Texas 78712, USA

[*]*adunn@mail.utexas.edu*

Abstract: Here we demonstrate that a mode-locked ytterbium fiber laser for two-photon fluorescence microscopy can be built for $13,000. The laser emits at a wavelength of 1060 nm with a usable average power of 1 W at a repetition rate of 40 MHz and a compressed pulse width of 81 fs at the sample. The laser is used to obtain deep *in vivo* two-color images of layer-V pyramidal neurons expressing YFP and vasculature labelled with Texas Red at depths up to 900 μm. The sub-1 μm features of dendritic spines can be resolved at a 200 μm depth.

OCIS codes: (140.4050) Mode-locked lasers; (170.3880) Medical and biological imaging; (190.4180) Multiphoton processes.

References and links

1. W. Denk, J. H. Strickler, and W. W. Webb, "Two-photon laser scanning fluorescence microscopy," Science **248**(4951), 73–76 (1990).
2. J. Grutzendler, N. Kasthuri, and W.-B. Gan, "Long-term dendritic spine stability in the adult cortex," Nature **420**(6917), 812–816 (2002).
3. M. Matsuzaki, N. Honkura, G. C. R. Ellis-Davies, and H. Kasai, "Structural basis of long-term potentiation in single dendritic spines," Nature **429**(6993), 761–766 (2004).
4. A. K. Dunn, V. P. Wallace, M. Coleno, M. W. Berns, and B. J. Tromberg, "Influence of optical properties on two-photon fluorescence imaging in turbid samples," Appl. Opt. **39**(7), 1194–1201 (2000).
5. M. Oheim, E. Beaurepaire, E. Chaigneau, J. Mertz, and S. Charpak, "Two-photon microscopy in brain tissue: parameters influencing the imaging depth," J. Neurosci. Methods **111**(1), 29–37 (2001).
6. M. Drobizhev, S. Tillo, N. Makarov, T. E. Hughes, and A. Rebane, "Absolute two-photon absorption spectra of orange and red fluorescent proteins," J. Phys. Chem. B **113**, 855–859 (2009).
7. M. Drobizhev, N. S. Makarov, S. E. Tillo, T. E. Hughes, and A. Rebane, "Two-photon absorption properties of fluorescent proteins," Nat. Methods **8**(5), 393–399 (2011).
8. K. Taira, T. Hashimoto, and H. Yokoyama, "Two-photon fluorescence imaging with a pulse source based on a 980-nm gain-switched laser diode," Opt. Express **15**(5), 2454–2458 (2007).
9. R. Kawakami, K. Sawada, A. Sato, T. Hibi, Y. Kozawa, S. Sato, H. Yokoyama, and T. Nemoto, "Visualizing hippocampal neurons with in vivo two-photon microscopy using a 1030 nm picosecond pulse laser," Sci. Rep. **3**, 1014 (2013).
10. C. Xu and F. W. Wise, "Recent advances in fibre lasers for nonlinear microscopy," Nat. Photonics **7**(11), 875–882 (2013).
11. M. E. Fermann and I. Hartl, "Ultrafast fibre lasers," Nat. Photonics **7**(11), 868–874 (2013).
12. D. U. Kim, H. Song, W. Song, H.-S. Kwon, M. Sung, and D. Y. Kim, "Two-photon microscopy using an Yb(3+)-doped fiber laser with variable pulse widths," Opt. Express **20**(11), 12341–12349 (2012).
13. J. R. Unruh, E. S. Price, R. G. Molla, L. Stehno-Bittel, C. K. Johnson, and R. Hui, "Two-photon microscopy with wavelength switchable fiber laser excitation," Opt. Express **14**(21), 9825–9831 (2006).
14. S. Tang, J. Liu, T. B. Krasieva, Z. Chen, and B. J. Tromberg, "Developing compact multiphoton systems using femtosecond fiber lasers," J. Biomed. Opt. **14**(3), 030508 (2009).
15. A. Chong, W. H. Renninger, and F. W. Wise, "All-normal-dispersion femtosecond fiber laser with pulse energy above 20 nJ," Opt. Lett. **32**(16), 2408–2410 (2007).
16. J. An, D. Kim, J. W. Dawson, M. J. Messerly, and C. P. J. Barty, "Grating-less, fiber-based oscillator that generates 25 nJ pulses at 80 MHz, compressible to 150 fs," Opt. Lett. **32**(14), 2010–2012 (2007).
17. K. Kieu, W. H. Renninger, A. Chong, and F. W. Wise, "Sub-100 fs pulses at watt-level powers from a dissipative-soliton fiber laser," Opt. Lett. **34**(5), 593–595 (2009).
18. M. Hofer, M. E. Fermann, F. Haberl, M. H. Ober, and A. J. Schmidt, "Mode locking with cross-phase and self-

phase modulation," Opt. Lett. **16**(7), 502–504 (1991).

19. A. Chong, W. H. Renninger, and F. W. Wise, "Properties of normal-dispersion femtosecond fiber lasers," J. Opt. Soc. Am. B **25**(2), 140 (2008).
20. C. V. Shank, R. L. Fork, R. Yen, R. H. Stolen, and W. J. Tomlinson, "Compression of femtosecond optical pulses," Appl. Phys. Lett. **40**(9), 761–763 (1982).
21. C. Xu, J. Guild, W. Webb, and W. Denk, "Determination of absolute two-photon excitation cross sections by in situ second-order autocorrelation," Opt. Lett. **20**(23), 2372 (1995).
22. S. M. S. Kazmi, A. J. Salvaggio, A. D. Estrada, M. A. Hemati, N. K. Shaydyuk, E. Roussakis, T. A. Jones, S. A. Vinogradov, and A. K. Dunn, "Three-dimensional mapping of oxygen tension in cortical arterioles before and after occlusion," Biomed. Opt. Express **4**(7), 1061–1073 (2013).
23. C. J. Schrandt, S. M. S. Kazmi, T. A. Jones, and A. K. Dunn, "Chronic monitoring of vascular progression after ischemic stroke using multiexposure speckle imaging and two-photon fluorescence microscopy," J. Cereb. Blood Flow Metab. **35**(6), 933–942 (2015).
24. F. Bestvater, E. Spiess, G. Stobrawa, M. Hacker, T. Feurer, T. Porwol, U. Berchner-Pfannschmidt, C. Wotzlaw, and H. Acker, "Two-photon fluorescence absorption and emission spectra of dyes relevant for cell imaging," J. Microsc. **208**(2), 108–115 (2002).
25. E. Spiess, F. Bestvater, A. Heckel-Pompey, K. Toth, M. Hacker, G. Stobrawa, T. Feurer, C. Wotzlaw, U. Berchner-Pfannschmidt, T. Porwol, and H. Acker, "Two-photon excitation and emission spectra of the green fluorescent protein variants ECFP, EGFP and EYFP," J. Microsc. **217**(3), 200–204 (2005).
26. E. Beaurepaire, M. Oheim, and J. Mertz, "Ultra-deep two-photon fluorescence excitation in turbid media," Opt. Commun. **188**(1-4), 25–29 (2001).
27. P. Theer, M. T. Hasan, and W. Denk, "Two-photon imaging to a depth of 1000 microm in living brains by use of a Ti:Al₂O₃ regenerative amplifier," Opt. Lett. **28**(12), 1022–1024 (2003).
28. A. Schönle and S. W. Hell, "Heating by absorption in the focus of an objective lens," Opt. Lett. **23**(5), 325–327 (1998).
29. D. Kobat, M. E. Durst, N. Nishimura, A. W. Wong, C. B. Schaffer, and C. Xu, "Deep tissue multiphoton microscopy using longer wavelength excitation," Opt. Express **17**(16), 13354–13364 (2009).
30. F. Bevilacqua, D. Piguet, P. Marquet, J. D. Gross, B. J. Tromberg, and C. Depeursinge, "In vivo local determination of tissue optical properties: applications to human brain," Appl. Opt. **38**(22), 4939–4950 (1999).
31. N. Nishimura, C. B. Schaffer, B. Friedman, P. S. Tsai, P. D. Lyden, and D. Kleinfeld, "Targeted insult to subsurface cortical blood vessels using ultrashort laser pulses: three models of stroke," Nat. Methods **3**(2), 99–108 (2006).
32. D. Kobat, N. G. Horton, and C. Xu, "In vivo two-photon microscopy to 1.6-mm depth in mouse cortex," J. Biomed. Opt. **16**(10), 106014 (2011).
33. N. G. Horton, K. Wang, D. Kobat, C. G. Clark, F. W. Wise, C. B. Schaffer, and C. Xu, "In vivo three-photon microscopy of subcortical structures within an intact mouse brain," Nat. Photon. **7**, 205–209 (2013).
34. S. Lefrançois, K. Kieu, Y. Deng, J. D. Kafka, and F. W. Wise, "Scaling of dissipative soliton fiber lasers to megawatt peak powers by use of large-area photonic crystal fiber," Opt. Lett. **35**(10), 1569–1571 (2010).
35. M. Baumgartl, F. Jansen, F. Stutzki, C. Jauregui, B. Ortaç, J. Limpert, and A. Tünnermann, "High average and peak power femtosecond large-pitch photonic-crystal-fiber laser," Opt. Lett. **36**(2), 244–246 (2011).

1. Introduction

First developed in early 1990's, two-photon microscopy is a powerful optical sectioning technique ideal for deep imaging of biological samples with submicron resolution [1]. The field of neuroscience saw a number of discoveries enabled by this technique [2,3]. The critical enabling tool for two-photon microscopy has been the ultrafast laser, typically <200 fs in pulse duration and emitting in the near infrared region >750 nm. For the past two decades, titanium-doped sapphire (Ti:S) lasers have been the industry standard for deep two-photon microscopy due to relatively robust optical design, high stability, high output power, and wide wavelength tuning (700-1000 nm) over a range accessible to most standard dyes. However, the system cost and complexity of these lasers typically limits their use to specialized labs, or as shared resources. Furthermore, at the upper limit of the tuning range (1000 nm) the output power typically degrades four-fold. It is well known that a longer excitation wavelength allows significantly deeper penetration into tissues [4,5] and offers a broad range of usable fluorescence proteins, many of which have a peak two-photon cross-section between 900 and 1100 nm [6,7]. To better investigate intact neurons and vasculature in a living mouse, it will be necessary to utilize light sources that offer deeper imaging than Ti:S lasers and with emission wavelengths that better overlap with the new generation of fluorescent proteins.

Alternatives to the Ti:S laser for biological microscopy have been explored in the past decade. A gain switched laser emitting at 980 nm was demonstrated for two-photon imaging an *ex vivo* mouse tissue [8]. Another study used a semiconductor based laser and amplifier system with a 5 ps pulse to image neurons labelled with eYFP *in vivo* [9]. Of the alternatives

to Ti:S laser systems, the fiber laser is potentially the most promising. Fiber lasers offer excellent pump absorption efficiency, high pulse energy, entirely passive mode-locking, and no need for active cooling [10,11]. Several groups have demonstrated two-photon imaging with fiber laser systems. One group utilized a homebuilt system with grating compressor to obtain pulse widths down to 384 fs with 80 mW average power [12]. Commercial fiber lasers with photonic crystal fiber have been employed for widely tunable systems [13], and for fiber delivery of femtosecond pulses to the sample [14]. Previous demonstrations of homebuilt and commercial fiber lasers have shown a great potential to be used as a low cost alternative to the Ti:S laser for *in vivo* imaging, however their pulse energy and average power is not sufficient to be used for deep *in vivo* brain imaging.

Recently, fiber lasers making use of the All Normal Dispersion (ANDi) design have allowed for power scaling up to 20 nJ pulse energy [15], but the use of a single mode pump laser limits the usable output to an average power of only 200 mW. A further improvement to the ANDi design enabled 10 times scaling of average power by switching to a multimode pumped laser and double clad gain fiber [16,17]. Despite the relatively simple optical design of the ANDi laser, it has seen limited use in two-photon microscopy systems. In this report we describe the performance of a double clad multimode-pumped ANDi ytterbium fiber laser, built in our lab, for deep-tissue *in vivo* brain imaging. We demonstrate that a robust and stable system can be built from entirely off the shelf commercial components for only $13,000, or approximately 1/10th the cost of a commercial Ti:S laser system. We characterize the laser to have a central wavelength of 1060 nm, with a 40 nm bandwidth. The laser emits 8 ps pulses that can be extracavity compressed to 81 fs. Two-photon imaging is demonstrated at depths up to 900 µm in an intact living mouse brain with YFP labelled layer-V neurons and Texas Red perfused vasculature.

2. Materials and methods

2.1 Fiber laser design

The self-starting mode-locked operation of the laser is based upon the non-linear polarization rotation effect [18,19]. Typical fiber laser designs utilize a single mode core with single mode pump which limits the usable output power to approximately 200 mW [15]. Here we adopt a multimode pump, double clad fiber design [17]. The gain medium lies within a 10 µm core large-mode area double clad fiber (YDF) (YB1200-10/125DC, nLIGHT Photonics), in this region the pump light from a multimode diode ($\lambda = 976$ nm) travels within the cladding of the YDF and is absorbed through chance encounters with the ytterbium-doped core of the fiber. This design allows scaling of the output power to 30 nJ pulses with uncompressed average powers of 1.2 W at a repetition rate of 40 MHz.

The laser is a ring cavity as seen in Fig. 1 with a total fiber cavity length of approximately 4.8 m and a small free space portion. The gain medium consists of 2.5 m of ytterbium-doped double clad fiber (YDF) followed by a pigtailed collimator (F220FC-1064, Thorlabs) with 0.8 m of HI1060 fiber. High power patch cable with a mechanically cleaved air gap (SMJ-A3HPC-X-1060-6/125-1-3, Oz Optics) is used to prevent damage during mode-locked operation. A free space portion of the laser accomplishes several tasks: (1) polarization control with waveplates, (2) ejection of pulses via a polarizing beam splitter, (3) unidirectional cavity with an isolator, and (4) spectral tuning through a birefringent filter plate. A second collimator with 0.5 m of HI1060 fiber is spliced onto 0.5 m of un-doped double clad fiber (UDCF) on the signal line of a multimode pump combiner (MMC02112CC0A, 3SP Group). A 10 W multimode fiber coupled diode pump laser (L4-9897603-100B, JDSU) provides the energy for lasing. Another 0.5 m of UDCF follows the pump combiner and is spliced onto the YDF closing the ring cavity. To reduce loss in the cavity from the mismatched core sizes at the splice joints between HI1060 and DC fiber we splice ~2 cm of an 8 µm core fiber (SMF28e, Corning). A more detailed description of the build process can be found in Appendix A.
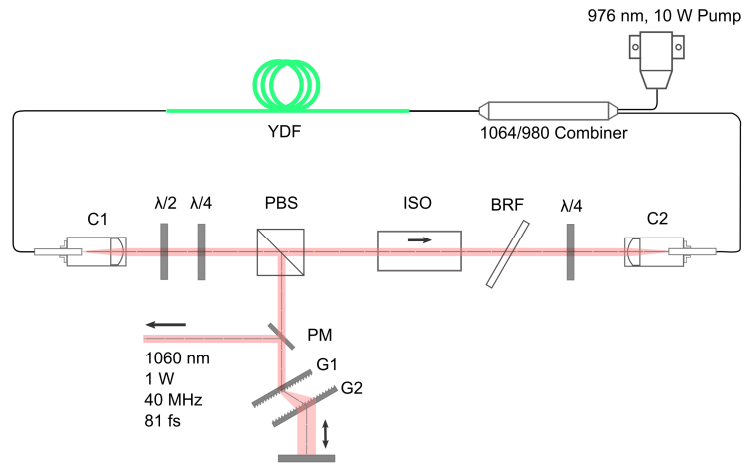
Fig. 1. Schematic of the mode-locked ytterbium fiber laser. The majority of the cavity lies within 4.8 meters of optical fiber. A free space portion is used to eject the pulses with a polarizing beam splitter (PBS). Half-wave and quarter-wave plates control the polarization rotation effect which initiates and sustains mode-locking. The birefringent filter plate (BRF) allows control of the spectral bandwidth in the cavity. G1 and G2 are transmission pulse compression gratings, PM is pick-off mirror, C1 and C2 are fiber collimators.

The spatial output of the fiber laser can be directly characterized by the light exiting from a single mode fiber collimator, C1 in Fig. 1. These collimators (F220FC-1064, Thorlabs) have an average beam quality factor, $M^2 = 1.1$, as characterized by the manufacturer. The divergence angle was calculated from ray optics to be 0.5 mrad, while the beam size is 2.4 mm in diameter.

External to the cavity is a double pass, grating pair compressor to compensate for the large dispersion introduced by the cavity [20]. The light is diffracted by two transmission diffraction gratings with grating pitch of 1000 lines/mm (LSFSG-1000-3212-94, LightSmyth). The path is folded onto itself and picked off by a mirror to be reflected into the microscope setup.

2.2 Characterization of laser

The laser achieves full output mode-locked operation at 4.5 W pump power and is able to maintain stability over an entire animal experiment duration, typically 4 hours. The longest consecutive time the laser was operated was for 10 hours, over which it remained stably mode-locked. The average power output directly from the cavity is 1.2W, after a four pass transmission grating compressor the usable power is 1 W.
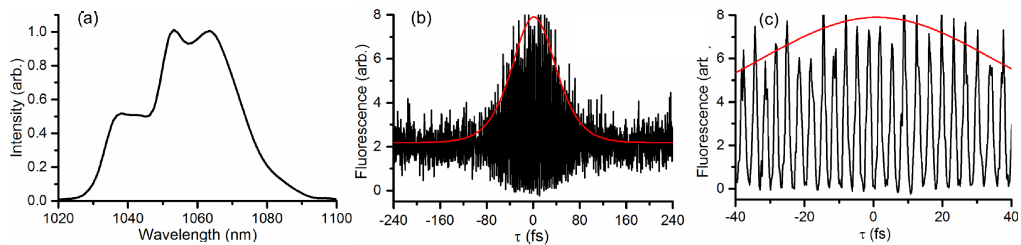

Fig. 2. (a) Emission spectrum of the mode-locked ytterbium laser. (b) Autocorrelation trace of the compressed pulse at the sample measured by *in situ* autocorrelation. The measured pulse width was found to be 127 fs full-width half max. Assuming a sech^2 pulse shape, the estimated pulse width is 81 fs. (c) Zoomed view of autocorrelation trace.

The spectral output was measured with a commercial spectrometer (AvaSpec-256-NIR1.7, Avantes) and found to be 40 nm bandwidth centered at 1060 nm [Fig. 2(a)]. The

pulse width at the sample was characterized by an *in situ* second-order autocorrelation technique [21] [Fig. 2(b)]. The pulse is long upon exiting the cavity (8 ps). With the external grating pair the pulse can be compressed down to 81 fs. It was found that a grating spacing of 20 mm provided the optimal pulse compression at the sample. The pulse is not transform limited because of large higher-order dispersion introduced by several meters of fiber cavity length [17].

2.3 Two-photon microscope

Two-photon laser scanning microscopy was performed on a custom built upright microscope for animal imaging [22] [Fig. 3(a)]. The laser is expanded with a two lens telescope assembly before being projected onto an xy-galvo mirror pair (6125H, Cambridge Tech.). A scan (25 mm) and tube lens (125 mm) are used to reimage the scanned laser onto the back aperture of the microscope objective (XLUMPLFLN 20 × 0.95 NA, Olympus). Fluorescence light is epi-collected and reflected towards the detectors by a dichroic mirror, DM1 (FF775-Di01-25x36, Semrock). The detectors are 5 mm area, short working distance, uncooled PMTs (H10770PB-40, Hamamatsu Photonics). A dichroic filter, DM2 separates emitted light into two channels. Emission filters are placed directly in front of the PMTs, corresponding to green (FF01-534/42-25, Semrock) for YFP, and red (FF01-534/42-25, Semrock) for Texas Red. The analog waveform from each PMT is sent to a current preamplifier before being digitized by a PCI-based DAQ (PCI-6353, National Instruments).
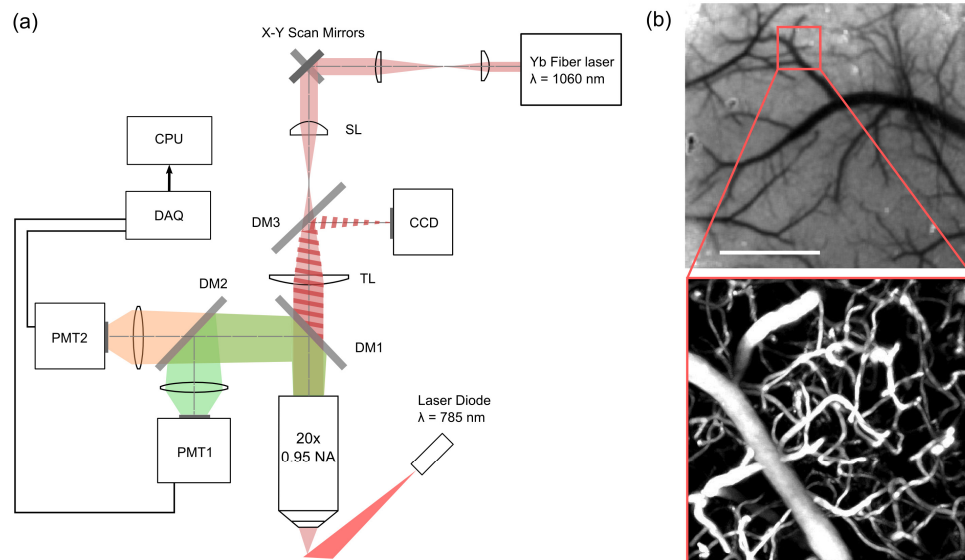

Fig. 3. (a) Custom two-photon instrument schematic. SL: scan lens, TL: tube lens, DM1, DM2, DM3: dichroic mirrors with transmission lines: T > 775 nm, T > 570 nm, and T > 795 nm, respectively (b) Laser speckle contrast image of the mouse craniotomy. The scale bar is 800 µm. (zoomed view: a representative two-photon maximum intensity z-projection of a 400 × 400 × 200 µm³ stack. The vessels are perfused with Texas Red.

Laser speckle contrast imaging (LSCI) was used to locate the optimal location to record two-photon image stacks [23]. At the start of an experiment, a laser speckle contrast image was taken [Fig. 3(b)] using a laser diode (λ = 785 nm) and a CCD camera through the same objective as used for imaging. Following the laser speckle imaging, two-photon microscopy was performed.

For a typical experiment, we used a 400 µm field of view and image resolution of 512 × 512 pixels, corresponding to a pixel size of 781 nm. The pixel integration time was 2.66 µs and images were acquired at 1 Hz. At the surface and up to 700 µm 5 frame averaging was used, while at depths greater than 700 µm 10 frame averaging was used.

2.4 Animal procedures

All animal procedures were reviewed and approved by the University of Texas at Austin Institutional Animal Care and Use Committee (protocol number AUP-2015-00011) and were conducted in strict accordance with the Guide for the Care and Use of Laboratory Animals (published by NIH), the Public Health Service Policy on Humane Care and Use of Laboratory Animals, and the Animal Welfare Act and Animal Welfare Regulations.

2.4.1 Chronic preparation

A genetically modified C57BL/6 mouse (female, 20-g) expressing yellow fluorescent protein in layer V pyramidal neurons was anesthetized using 5 percent isoflurane (VetOne). Eye ointment was applied and the temperature was monitored and kept constant at 37.5°C with a feedback heating plate (World Precision Instruments Inc., Sarasota, FL). Next, Carprofen (5mg/kg, subcutaneous) and dexamethasone sodium phosphate (2mg/kg, intramuscular) were administered to control inflammation. The mouse was transferred into a stereotaxic frame. The mouse head was cleaned with ethanol, lidocaine was applied under the head skin and the skin from the top of the head was removed using scissors. The scalp was exposed and a ~4 mm circular diameter portion of the skull was removed (center located at 3 mm lateral and 3 mm caudal from bregma). A 5 mm sterile glass #1.5 cover slip (502040, World Precision Instruments) was placed over the craniotomy and glued to the skull using cyanoacrylate and dental cement. After sealing the craniotomy, the animal was removed from anesthesia and allowed to recover for two weeks. Carprofen injections were given daily for the next 2 days after surgical procedure. The procedure was performed using autoclaved tools and materials.

2.4.2 Imaging session

For the imaging sessions the YFP mouse was placed into the stereotaxic frame, kept under isoflurane anesthesia, body temperature was maintained at 37.5°C and 0.1 mL subcutaneous injections of 5% (w/v) glucose in physiological saline were applied every hour. After verifying that the mice was under anesthesia by a lack of the paw pinch reflex, blood plasma was labeled via an intraorbital injection of 5% (w/v) Texas Red-dextran (D1864, Invitrogen) dissolved in physiological saline.

3. Results and discussion

Deep brain imaging using the custom 1060 nm fiber laser was performed in an anesthetized YFP mouse with a previously implanted cranial window. Images of the brain were obtained using LSCI for reference followed by two-photon microscopy. 3D images stacks were taken with 5 μm separation between image planes. A power of 20 mW at the objective back aperture was used for surface level imaging, while 200 mW was needed for depths of >700 μm. A variable neutral density filter allowed for manual control of laser power at varying depths. A comparatively higher power was required for surface level imaging due to low objective transmission (~65% at 1060 nm) and off peak excitation of Texas Red and YFP (<60% relative to peak) [24,25]. It is possible that using a fluorophore with a better matched 2P cross-section at 1060 nm would allow for a lower excitation power for surface level imaging.

Images of vasculature perfused with Texas Red and neurons expressing YFP, as shown in Fig. 4, were measured to depths up to 750 μm. Rendering of the 3D stack data is performed with a 3D visualization software (Aviso standard, VSG). Figure 4(c) shows a merged plane projection images at various depths through the stack. Each plane is a maximum intensity z-projection image of the nearest 10 μm. From [Fig. 4(b)], we can observe the progression of neural structure from the top ~100 μm of branching dendrites down to the neuron bodies at depths of 700-800 μm.
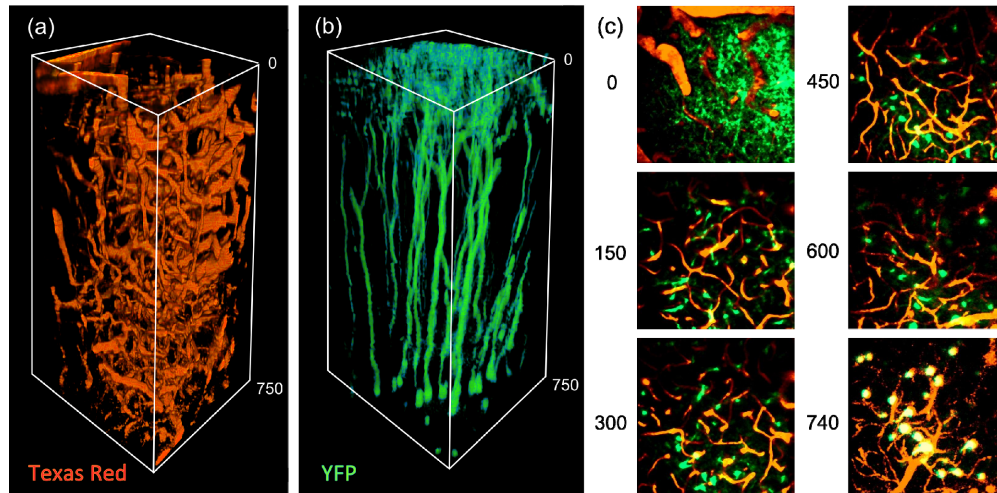
Fig. 4. (a and b) Image stack of dimensions $400 \times 400 \times 750$ μm^3 taken with two-photon laser scanning microscopy labeling for (a) microvasculature with Texas Red, and (b) Neurons expressing YFP. (c) 2D z-projections at various depths through the stack, the image at each plane is a maximum intensity projection of the nearest 10 μm.

We further investigate the neuron structural imaging capability of the laser and compare performance to that of a commercial Ti:S laser tuned to 920 nm. Two stacks were recorded down to 900 μm in two different mice using a commercial Ti:S laser (Mira 900, Coherent) and the custom fiber laser. For the fiber laser, the same previously mentioned back aperture excitation powers were used at the surface (20 mW) and at depth (200 mW), while the Ti:S laser used a proportionally scaled excitation pulse energy to account for the decreased 2P cross-section of YFP at 920 nm. The Ti:S excitation power ranged from 30 mW at the surface to 380 mW at 900 μm depth. The same frame averaging conditions were performed with each laser. In both cases we observe neuron bodies at depths around 700 μm [Fig. 5(a)]. Although, with the commercial Ti:S laser, past ~650 μm the background signal increased dramatically. With the Ti:S at 900 μm the signal-to-noise ratio (SNR) was so low that no structure could be resolved, whereas with the fiber laser SNR remained acceptable throughout the 900 μm image. Although experimental conditions can vary, in this specific case we see that the 1060 nm fiber laser offers superior deep imaging capability to that of a Ti:S laser tuned near the end of its standard operating range, 920 nm. The difference in excitation wavelengths between the two lasers has a notable impact on the imaging performance, however additional differences such as shorter pulse width (81 fs vs. 150 fs), and lower auto-fluorescence from the fiber laser are likely significant factors in the improved imaging depth.

Upon zooming in to a single apical dendrite at 200 μm depth with the fiber laser, it is possible to resolve single dendritic spines [Fig. 5(b)]. In this case our image resolution was no longer limited by the pixel size (64 nm), but instead, by optical diffraction (~350 nm), We observe that the thin features of dendritic spines are still easily resolvable using 1060 nm light, even to depths of 200 μm. Going to depths further than 900 μm yielded no signal even with increasing laser power. Although YFP had acceptable SNR with 10 frame averaging at 900 μm [Fig. 5(c)], the signal level decayed past that point, indicating that a practical depth limit had been reached. It is likely that the poor SNR past 900 μm was due to loss of signal rather than an overwhelming noise from out of focus fluorescence. With a higher peak power, a brighter fluorophore, or better collection optics, it should be possible to obtain even deeper imaging with the 1060 nm wavelength. For example, using a fluorescent protein such as tdTomato would allow for even deeper imaging due to its significantly greater two-photon cross-section around 1060 nm [6].
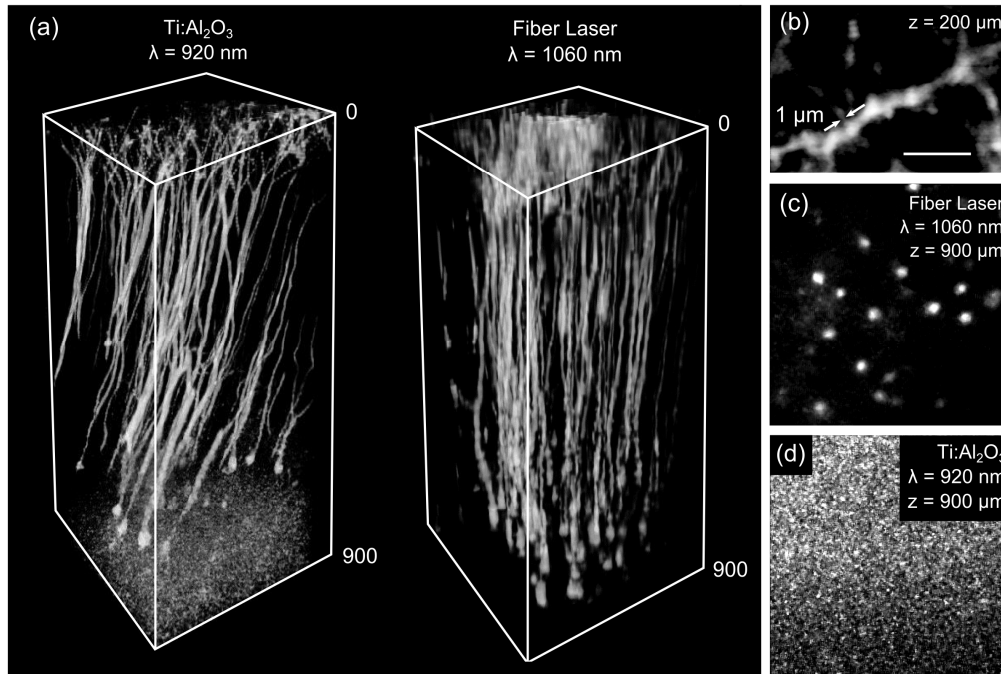
Fig. 5. (a) Deep imaging comparison between a commercial Ti:S laser tuned to 920 nm and the custom built 1060 nm fiber laser. Image dimensions $400 \times 400 \times 900$ μm³. Fluorescence stacks are pyramidal neurons expressing YFP taken in two separate mice. (b) A zoomed in view of a dendrite at 200 μm depth taken with the fiber laser. Single dendritic spines can be visualized with sub 1 μm features. Scale bar is 8 μm. (c) An image of pyramidal neuron bodies at 900 μm depth taken with the fiber laser. (d) An image at 900 μm depth taken with a commercial Ti:S laser, neuron structures cannot be resolved.

This work demonstrates that with our microscopy setup and custom laser we can achieve a practical imaging depth of 900 μm in an intact live mouse brain, which is superior to most standard Ti:S laser oscillators operating at 800 nm [5], and comparable to studies performed with Ti:S regenerative amplifiers [26,27]. Comparing the specifications of the demonstrated 1060 nm laser and modern Ti:S lasers that are tunable out to 1060 nm, it is clear that the fiber laser offers higher performance at the 1060 nm wavelength. With $8 \times$ higher pulse energy and a shorter pulse width (81 fs vs. 140 fs), the fiber laser has a peak power well over an order of magnitude above Ti:S systems. Given the difference in peak power the fiber laser should be capable of achieving significantly deeper imaging than a modern Ti:S tuned to the same wavelength. In terms of pulse repetition rate, duty cycle, and photodamage the fiber laser should offer comparable performance to that of a Ti:S laser. Tissue heating from water absorption can be a concern when using longer excitation wavelengths. Despite almost 3 orders of magnitude higher water absorption at 1060 nm versus 800 nm, it is unlikely that tissue damage due to heating is increased. There has been shown to be insignificant heat accumulation in tissue samples (<0.2 K at 800 nm) with femtosecond pulsed lasers [28], due to comparatively low pulse energy. Femtosecond pulses do not generate sufficient absorption over the image area to increase temperature by 1K within the sample even with wavelengths out to 1300 nm where absorption is much higher [29]. Furthermore, even though the absorption of water is significantly higher at 1060 nm versus 800 nm, the overall tissue absorption coefficient is within a factor of two due to the increased absorption of oxygenated and deoxygenated hemoglobin at 800 versus 1060 nm [30].

Although groups have demonstrated imaging as deep as 1 mm with a regenerative amplifier, it should be noted that regenerative amplifiers have as much as 100 times the pulse energy, and at 50 times lower duty cycle – the combination of which can lead to poor image

quality, slow acquisition, and tissue damage. Certain studies use regenerative amplifiers specifically to damage healthy brain tissue through optical breakdown effects with high pulse intensities [31]. With our setup, there was no damage to the surface of the brain through extravasation, or hemorrhaging even with the highest tested power of 500 mW at the back aperture.

Other groups have utilized lasers with even longer excitation wavelengths, in the range of 1200-1700 nm, that are capable of imaging to up to 1.6 mm in a living mouse brain. These systems are built upon either commercial OPOs [32], or are a mix of custom and commercial products [33]. We emphasize that our system is entirely custom built, and for an order of magnitude lower cost. Yet, our fiber laser can achieve imaging depth close to that of the more complicated systems such as OPOs, or Ti:S regenerative amplifiers.

This specific laser embodiment provides sufficient pulse energy, 30 nJ, and average uncompressed power, 1.2 W, to image deep in highly scattering tissues. Although, in practice, it is possible to further scale the average power up to 2.4 W by increasing the repetition rate to 80 MHz [16]. Power scaling beyond 30 nJ pulse energy has been demonstrated by using large-mode-area photonic crystal fibers to manage instability from higher-order modes [34,35]. However, these systems typically suffer from increased alignment complexity due to free space coupled pump light.

4. Conclusion

In this work we detail the construction and application of an all normal dispersion mode-locked ytterbium fiber laser for two-photon microscopy. The laser achieves stable and self-starting mode-locking at 1060 nm center wavelength with 81 fs compressed pulses and a rate of 40 MHz. We use this custom built laser to demonstrate *in vivo* two-photon imaging of the intact brain of a living mouse down to a depth of 900 μm. Based on the simplicity and low cost of this laser design we believe it will be a highly valuable tool for labs that cannot afford traditional Ti:S laser systems. The cost alone would be a large draw for any neuroscience groups wishing to study intact neuron structure and function *in vivo*, where a Ti:S laser system would be otherwise impractical or not feasible. Furthermore, the longer wavelength allows deeper penetration into tissue, and access to a wider range of fluorescent proteins than possible with Ti:S lasers emitting between 700 and 900 nm. It is clear that the fiber laser approach has numerous benefits over traditional femtosecond mode-locked lasers and we expect to see more labs adopt fiber lasers for their multiphoton microscopy research in the near future.

Appendix A: description of laser build

A.1 Procedure for laser build

Refer to Table 1 for a list of the components used in this build. Fusion splicing of the fiber components is the first completion milestone, with laser alignment and mode-locking being the second and third milestones, respectively. Many of the fiber components are of differing core size and, for this reason, should be spliced using a core-alignment fusion splicer as opposed to V-groove. The splicer used for this build was a FFS200PM from Vytran. First, the HI1060 patchcord attached to the collimators, C1 and C2 in Fig. 1, are spliced to a small section of SMF fiber (<2 cm). This intermediate splice allows a taper in core size from 5.2 μm up to 8.2 μm to reduce splice loss (<0.2 dB typical). The C1 fiber assembly (containing 0.8 m of HI1060 patch cable and 2 cm of SMF fiber) is spliced to the 2.5 m section of ytterbium doped gain fiber, typical splice loss for the entire assembly should reach 0.5 dB. Next, both assemblies, C1 and C2 are spliced to the multimode combiner output and input signal lines, respectively. The length of the input and output signal lines are both 0.5 m. The final splice is the 105 μm core multimode fiber coupled pump laser; no specific target fiber length is needed. The fiber output from the pump laser is spliced to either one of the multimode input fibers of the combiner unit, the other input line can be left unused. A (1+1)x1 combiner may also be used.

Once all of the fiber splices have been completed the alignment process can begin. The first step in laser alignment is to close the circular cavity and obtain lasing, this is accomplished by aligning the output collimator, C1, to the input collimator, C2, through the isolator, ISO. An isolator should always be used during alignment for stability and to avoid damaging the components. The waveplates and birefringent plate are not necessary to achieve lasing. The pump power should be set to a value near the lasing threshold, for this laser cavity the lasing threshold is at approximately 1.5W of pump power. Upon lasing, the waveplates and BRF can be inserted into their respective locations as described by Fig. 1. The alignment should be adjusted again to maximize output power. The BRF should be placed near the Brewster angle. Mode-locking can be achieved by systematically rotating the waveplates and BRF at a high enough pump power for non-linear polarization evolution to occur. The mode-locking threshold for this laser is approximately 3.5 W of pump power. The specific angles for waveplates and the BRF that achieve mode-locking will vary between different builds. During rotation of the waveplates to achieve mode-locking we never noticed damage to the high power patch cable collimators, even with higher pump powers of 5-6 W. With standard epoxy polished terminated fiber, damage occurred during rotation of waveplates to both the input and output end-faces of the fiber collimators.

Table 1. Summary of select components used in laser build[a]

Description	Supplier	Manufacturer's Part #	Price	Qty.
10 W, 976 nm Laser Diode Pump	JDS Uniphase	L4-9897603-100B	$325	1
20 A Laser Diode Driver	Arroyo Instruments	4320	$1995	1
28W TEC Driver	Arroyo Instruments	585-04-08	$695	1
TEC Laser Mount	Arroyo Instruments	207	$595	1
(2 + 1)x1 Multimode Combiner	3SP Group	MMC02112CC0A	$460	1
Ytterbium-Doped LMA Double Clad Fiber	Thorlabs	YB1200-10/125DC	$168	3
High-power HI1060 Patchcord	Oz Optics	SMJ-A3HPC,X-1060-6/125-1-3	$189	2
1064 nm, FC/PC Fiber Collimation Pkg.	Thorlabs	F220FC-1064	$134	2
Polarizing Beamsplitter Cube, 900-1300 nm	Thorlabs	CM05-PBS203	$255	1
Achromatic Quarter Waveplate, 690-1200 nm	Thorlabs	AQWP05M-980	$783	2
Achromatic Half Waveplate, 690-1200 nm	Thorlabs	AHWP05M-980	$783	1
1 mm thk. Quartz Birefringent Plate	OFR	BF-16-1.00	$275	1
60 W Max, 1064 nm Isolator	Thorlabs	IO-5-1064-HP	$2435	1
High-Precision Rotation Mount for Ø1" Optics	Thorlabs	PRM1	$260	4
1000 line/mm Transmission Grating	LightSmyth	LSFSG-1000-3212-94	$395	2
Breadboard, 2' x 1.5′ x 2.2", 1/4"-20 Taps	Newport	PBG12118	$654	1

[a]Opto-mechanical components have been omitted and can be selected based on user preference.

Acknowledgments